Wavelet-based Image Compression

Sub-chapter of CRC Press book: *Transforms and Data Compression*

James S. Walker
Department of Mathematics
University of Wisconsin–Eau Claire
Eau Claire, WI 54702–4004

Phone: 715–836–3301
Fax: 715–836–2924
e-mail: walkerjs@uwec.edu

1 Image compression

There are two types of image compression: *lossless* and *lossy.* With lossless compression, the original image is recovered exactly after decompression. Unfortunately, with images of natural scenes it is rarely possible to obtain error-free compression at a rate beyond 2:1. Much higher compression ratios can be obtained if some error, which is usually difficult to perceive, is allowed between the decompressed image and the original image. This is lossy compression. In many cases, it is not necessary or even desirable that there be error-free reproduction of the original image. For example, if some noise is present, then the error due to that noise will usually be significantly reduced via some denoising method. In such a case, the small amount of error introduced by lossy compression may be acceptable. Another application where lossy compression is acceptable is in fast transmission of still images over the Internet.

We shall concentrate on wavelet-based lossy compression of grey-level still images. When there are 256 levels of possible intensity for each pixel, then we shall call these images 8 bpp (bits per pixel) images. Images with 4096 grey-levels are referred to as 12 bpp. Some brief comments on color images will also be given, and we shall also briefly describe some wavelet-based lossless compression methods.

1.1 Lossy compression

The methods of lossy compression that we shall concentrate on are the following: the *EZW* algorithm, the *SPIHT* algorithm, the *WDR* algorithm, and the *ASWDR* algorithm. These are relatively recent algorithms which achieve some of the lowest errors per compression rate and highest perceptual quality yet reported. After describing these algorithms in detail, we shall list some of the other algorithms that are available.

Before we examine the algorithms listed above, we shall outline the basic steps that are common to all wavelet-based image compression algorithms. The five stages of compression and decompression are shown in Figs. 1 and 2. All of the steps shown in the compression diagram are invertable, hence lossless, except for the *Quantize* step. Quantizing refers to a reduction of the precision of the floating point values of the wavelet transform, which are typically either 32-bit or 64-bit floating point numbers. To use less bits in the compressed transform—which is necessary if compression of 8 bpp or 12

bpp images is to be achieved—these transform values must be expressed with less bits for each value. This leads to rounding error. These approximate, quantized, wavelet transforms will produce approximations to the images when an inverse transform is performed. Thus creating the error inherent in lossy compression.

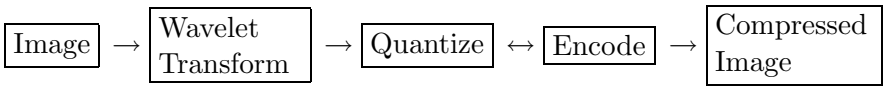

Figure 1: Compression of an image

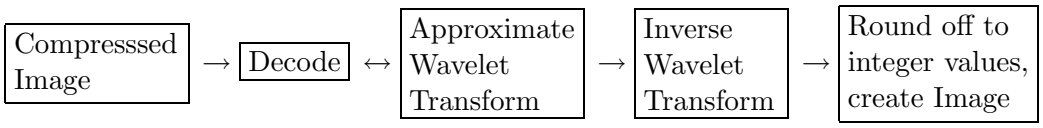

Figure 2: Decompression of an image

The relationship between the *Quantize* and the *Encode* steps, shown in Fig. 1, is the crucial aspect of wavelet transform compression. Each of the algorithms described below takes a different approach to this relationship.

The purpose served by the *Wavelet Transform* is that it produces a large number of values having zero, or near zero, magnitudes. For example, consider the image shown in Fig. 3(a), which is called *Lena*. In Fig. 3(b), we show a 7-level Daub 9/7 wavelet transform of the Lena image. This transform has been *thresholded*, using a threshold of 8. That is, all values whose magnitudes are less than 8 have been set equal to 0, they appear as a uniformly grey background in the image in Fig. 3(b). These large areas of grey background indicate that there is a large number of zero values in the thresholded transform. If an inverse wavelet transform is performed on this thresholded transform, then the image in Fig. 3(c) results (after rounding to integer values between 0 and 255). It is difficult to detect any difference between the images in Figs. 3(a) and (c).

The image in Fig. 3(c) was produced using only the $32,498$ non-zero values of the thresholded transform, instead of all $262,144$ values of the original

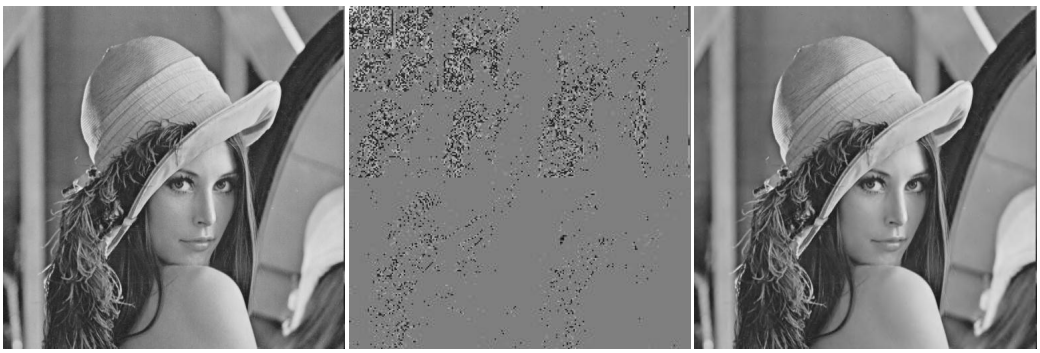

(a) (b) (c)

Figure 3: (a) *Lena* image, 8 bpp. (b) Wavelet transform of image, threshold = 8. (c) Inverse of thresholded wavelet transform, PSNR = 39.14 dB.

transform. This represents an 8:1 compression ratio. We are, of course, ignoring difficult problems such as how to transmit concisely the positions of the non-zero values in the thresholded transform, and how to encode these non-zero values with as few bits as possible. Solutions to these problems will be described below, when we discuss the various compression algorithms.

Two commonly used measures for quantifying the error between images are *Mean Square Error* (MSE) and *Peak Signal to Noise Ratio* (PSNR). The MSE between two images f and g is defined by

$$\text{MSE} = \frac{1}{N} \sum_{j,k} \left(f[j,k] - g[j,k] \right)^2 \tag{1}$$

where the sum over j, k denotes the sum over all pixels in the images, and N is the number of pixels in each image. For the images in Figs. 3(a) and (c), the MSE is 7.921. The PSNR between two (8 bpp) images is, in decibels,

$$\text{PSNR} = 10 \log_{10} \left(\frac{255^2}{\text{MSE}} \right). \tag{2}$$

PSNR tends to be cited more often, since it is a logarithmic measure, and our brains seem to respond logarithmically to intensity. Increasing PSNR represents increasing fidelity of compression. For the images in Figs. 3(a) and (c), the PSNR is 39.14 dB. Generally, when the PSNR is 40 dB or larger, then the two images are virtually indistinguishable by human observers. In this case, we can see that 8:1 compression should yield an image almost

identical to the original. The methods described below do in fact produce such results, with even greater PSNR than we have just achieved with our crude approach.

1	2	5	8	17	24	25	32
3	4	6	7	18	23	26	31
9	10	13	14	19	22	27	30
12	11	15	16	20	21	28	29
33	34	35	36	49	50	54	55
40	39	38	37	51	53	56	61
41	42	43	44	52	57	60	62
48	47	46	45	58	59	63	64

(a) 2-level

1	2	5	8	17	24	25	32
3	4	6	7	18	23	26	31
9	10	13	14	19	22	27	30
12	11	15	16	20	21	28	29
33	34	35	36	49	50	54	55
40	39	38	37	51	53	56	61
41	42	43	44	52	57	60	62
48	47	46	45	58	59	63	64

(b) 3-level

Figure 4: Scanning for wavelet transforms: zigzag through all-lowpass subband, column scan through vertical subbands, row scan through horizontal subbands, zigzag through diagonal subbands. (a) and (b): Order of scanned elements for 2-level and 3-level transforms of 8 by 8 image.

Before we begin our treatment of various "state of the art" algorithms, it may be helpful to briefly outline a "baseline" compression algorithm of the kind described in [1] and [2]. This algorithm has two main parts.

First, the positions of the significant transform values—the ones having larger magnitudes than the threshold T—are determined by scanning through the transform as shown in Fig. 4. The positions of the significant values are then encoded using a run-length method. To be precise, it is necessary to store the values of the *significance map:*

$$s(m) = \begin{cases} 0 & \text{if } |w(m)| < T \\ 1 & \text{if } |w(m)| \geq T, \end{cases} \tag{3}$$

where m is the scanning index, and $w(m)$ is the wavelet transform value at index m. From Fig. 3(b) we can see that there will be long runs of $s(m) = 0$. If the scan order illustrated in Fig. 4 is used, then there will also be long

runs of $s(m) = 1$. The positions of significant values can then be concisely encoded by recording sequences of 6-bits according to the following pattern:

$$\begin{aligned} 0\,a\,b\,c\,d\,e&: \text{ run of 0 of length } (a\,b\,c\,d\,e)_2 \\ 1\,a\,b\,c\,d\,e&: \text{ run of 1 of length } (a\,b\,c\,d\,e)_2. \end{aligned}$$

A lossless compression, such as Huffman or arithmetic compression, of these data is also performed for a further reduction in bits.

Second, the significant values of the transform are encoded. This can be done by dividing the range of transform values into subintervals (*bins*) and rounding each transform value into the midpoint of the bin in which it lies. In Fig. 5 we show the histogram of the frequencies of significant transform values lying in 512 bins for the 7-level Daub 9/7 transform of Lena shown in Fig. 3(b). The extremely rapid drop in the frequencies of occurrence of higher transform magnitudes implies that the very low-magnitude values, which occur much more frequently, should be encoded using shorter length bit sequences. This is typically done with either Huffman encoding or arithmetic coding. If arithmetic coding is used, then the average number of bits needed to encode each significant value in this case is about 1 bit.

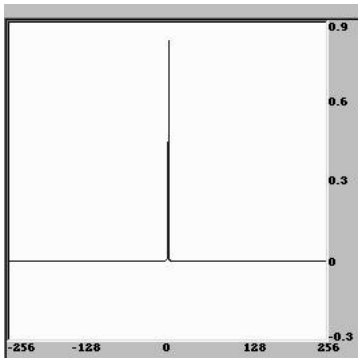

Figure 5: Histogram for 512 bins for thresholded transform of Lena

We have only briefly sketched the steps in this baseline compression algorithm. More details can be found in [1] and [2].

Our purpose in discussing the baseline compression algorithm was to introduce some basic concepts, such as scan order and thresholding, which are needed for our examination of the algorithms to follow. The baseline algorithm was one of the first to be proposed using wavelet methods [3]. It suffers

from some defects which later algorithms have remedied. For instance, with the baseline algorithm it is very difficult, if not impossible, to specify in advance the exact compression rate or the exact error to be achieved. This is a serious defect. Another problem with the baseline method is that it does not allow for progressive transmission. In other words, it is not possible to send successive data packets (over the Internet, say) which produce successively increased resolution of the received image. Progressive transmission is vital for applications that include some level of interaction with the receiver.

Let us now turn to these improved wavelet image compression algorithms. The algorithms to be discussed are the EZW algorithm, the SPIHT algorithm, the WDR algorithm, and the ASWDR algorithm.

1.2 EZW algorithm

The EZW algorithm was one of the first algorithms to show the full power of wavelet-based image compression. It was introduced in the groundbreaking paper of Shapiro [4]. We shall describe EZW in some detail because a solid understanding of it will make it much easier to comprehend the other algorithms we shall be discussing. These other algorithms build upon the fundamental concepts that were first introduced with EZW.

Our discussion of EZW will be focused on the fundamental ideas underlying it; we shall not use it to compress any images. That is because it has been superseded by a far superior algorithm, the SPIHT algorithm. Since SPIHT is just a highly refined version of EZW, it makes sense to first describe EZW.

EZW stands for *Embedded Zerotree Wavelet.* We shall explain the terms *Embedded,* and *Zerotree,* and how they relate to *Wavelet*-based compression. An embedded coding is a process of encoding the transform magnitudes that allows for progressive transmission of the compressed image. Zerotrees are a concept that allows for a concise encoding of the positions of significant values that result during the embedded coding process. We shall first discuss embedded coding, and then examine the notion of zerotrees.

The embedding process used by EZW is called *bit-plane encoding.* It consists of the following five-step process:

Bit-plane encoding

Step 1 (*Initialize*). Choose initial threshold, $T = T_0$, such that *all* transform values satisfy $|w(m)| < T_0$ and at least one transform value satisfies $|w(m)| \geq T_0/2$.

Step 2 (*Update threshold*). Let $T_k = T_{k-1}/2$.

Step 3 (*Significance pass*). Scan through insignificant values using baseline algorithm scan order. Test each value $w(m)$ as follows:

```
If |w(m)| ≥ T_k, then
    Output sign of w(m)
    Set w_Q(m) = T_k
Else if |w(m)| < T_k then
    Let w_Q(m) retain its initial value of 0.
```

Step 4 (*Refinement pass*). Scan through significant values found with higher threshold values T_j, for $j < k$ (if $k = 1$ skip this step). For each significant value $w(m)$, do the following:

```
If |w(m)| ∈ [w_Q(m), w_Q(m) + T_k), then
    Output bit 0
Else if |w(m)| ∈ [w_Q(m) + T_k, w_Q(m) + 2T_k), then
    Output bit 1
    Replace value of w_Q(m) by w_Q(m) + T_k.
```

Step 5 (*Loop*). Repeat steps 2 through 4.

This bit-plane encoding procedure can be continued for as long as necessary to obtain quantized transform magnitudes $w_Q(m)$ which are as close as desired to the transform magnitudes $|w(m)|$. During decoding, the signs and the bits output by this method can be used to construct an approximate wavelet transform to any desired degree of accuracy. If instead, a given compression ratio is desired, then it can be achieved by stopping the bit-plane encoding as soon as a given number of bits (a *bit budget*) is exhausted. In either case, the execution of the bit-plane encoding procedure can terminate at any point (not just at the end of one of the loops).

As a simple example of bit-plane encoding, suppose that we just have two transform values $w(1) = -9.5$ and $w(2) = 42$. For an initial threshold, we set $T_0 = 64$. During the first loop, when $T_1 = 32$, the output is the sign of $w(2)$, and the quantized transform magnitudes are $w_Q(1) = 0$ and $w_Q(2) = 32$. For the second loop, $T_2 = 16$, and there is no output from the significance pass. The refinement pass produces the bit 0 because $w(2) \in [32, 32 + 16)$. The quantized transform magnitudes are $w_Q(1) = 0$ and $w_Q(2) = 32$. During

the third loop, when $T_3 = 8$, the significance pass outputs the sign of $w(1)$. The refinement pass outputs the bit 1 because $w(2) \in [32+8, 32+16)$. The quantized transform magnitudes are $w_Q(1) = 8$ and $w_Q(2) = 40$.

It is not hard to see that *after n loops, the maximum error between the transform values and their quantized counterparts is less than* $T_0/2^n$. It follows that we can reduce the error to as small a value as we wish by performing a large enough number of loops. For instance, in the simple example just described, with seven loops the error is reduced to zero. The output from these seven loops, arranged to correspond to $w(1)$ and $w(2)$, is

$$\begin{array}{lccccccc} w(1): & & & - & 0 & 0 & 1 & 1 \\ w(2): & + & 0 & 1 & 0 & 1 & 0 & 0 \end{array}$$

Notice that $w(2)$ requires seven symbols, but $w(1)$ only requires five.

Bit-plane encoding simply consists of computing binary expansions—using T_0 as unit—for the transform values and recording *in magnitude order* only the significant bits in these expansions. Because the first significant bit is always 1, it is *not* encoded. Instead the sign of the transform value is encoded first. This coherent ordering of encoding, with highest magnitude bits encoded first, is what allows for progressive transmission.

Wavelet transforms are particularly well-adapted for bit-plane encoding.[1] This is because wavelet transforms of images of natural scenes often have relatively few high-magnitude values, which are mostly found in the highest level subbands. These high-magnitude values are first coarsely approximated during the initial loops of the bit-plane encoding. Thereby producing a low-resolution, but often recognizable, version of the image. Subsequent loops encode lower magnitude values and refine the high magnitude values. This adds further details to the image and refines existing details. Thus progressive transmission is possible, and encoding/decoding can cease once a given bit budget is exhausted or a given error target is achieved.

Now that we have described the embedded coding of wavelet transform values, we shall describe the zerotree method by which EZW transmits the positions of significant transform values. The zerotree method gives an implicit, very compact, description of the location of significant values by creating a highly compressed description of the location of insignificant values. For many images of natural scenes, such as the Lena image for example, insignificant values at a given threshold T are organized in zerotrees.

[1] Although other transforms, such as the block Discrete Cosine Transform, can also be bit-plane encoded.

To define a zerotree we first define a *quadtree.* A quadtree is a tree of locations in the wavelet transform with a root $[i, j]$, and its *children* located at $[2i, 2j]$, $[2i+1, 2j]$, $[2i, 2j+1]$, and $[2i+1, 2j+1]$, and each of their children, and so on. These *descendants* of the root reach all the way back to the 1^{st} level of the wavelet transform. For example, in Fig. 6(a), we show two quadtrees (enclosed in dashed boxes). One quadtree has root at index 12 and children at indices $\{41, 42, 47, 48\}$. This quadtree has two levels. We shall denote it by $\{12 \,|\, 41, 42, 47, 48\}$. The other quadtree, which has three levels, has its root at index 4, the children of this root at indices $\{13, 14, 15, 16\}$, and their children at indices $\{49, 50, \ldots, 64\}$. It is denoted by $\{4 \,|\, 13, \ldots, 16 \,|\, 49, \ldots, 64\}$.

Now that we have defined a quadtree, we can give a simple definition of a zerotree. *A zerotree is a quadtree which, for a given threshold T, has insignificant wavelet transform values at each of its locations.* For example, if the threshold is $T = 32$, then each of the quadtrees shown in Fig. 6(a) is a zerotree for the wavelet transform in Fig. 6(b). But if the threshold is $T = 16$, then $\{12 \,|\, 41, 42, 47, 48\}$ remains a zerotree, but $\{4 \,|\, 13, \ldots, 16 \,|\, 49, \ldots, 64\}$ is no longer a zerotree because its root value is no longer insignificant.

Zerotrees can provide very compact descriptions of the locations of insignificant values because it is only necessary to encode one symbol, R say, to mark the root location. The decoder can infer that all other locations in the zerotree have insignificant values, so *their locations are not encoded.* For the threshold $T = 32$, in the example just discussed, two R symbols are enough to specify all 26 locations in the two zerotrees.

Zerotrees can only be useful if they occur frequently. Fortunately, with wavelet transforms of natural scenes, the multiresolution structure of the wavelet transform does produce many zerotrees (especially at higher thresholds). For example, consider the images shown in Fig. 7. In Fig. 7(a) we show the 2^{nd} all-lowpass subband of a Daub 9/7 transform of the Lena image. The image 7(b) on its right is the 3^{rd} vertical subband produced from this all-lowpass subband, with a threshold of 16. Notice that there are large patches of grey pixels in this image. These represent insignificant transform values for the threshold of 16. These insignificant values correspond to regions of nearly constant, or nearly linearly graded, intensities in the image in 7(a). Such intensities are nearly orthogonal to the analyzing Daub 9/7 wavelets. Zerotrees arise for the threshold of 16 because in image 7(c)—the 2^{nd} all-lowpass subband—there are similar regions of constant or linearly graded intensities. In fact, it was precisely these regions which were smoothed and downsampled to create the corresponding regions in image 7(a). These re-

1	2	5	8	17	24	25	32
3	**4**	6	7	18	23	26	31
9	10	**13**	**14**	19	22	27	30
12	11	**15**	**16**	20	21	28	29
33	34	35	36	**49**	**50**	**54**	**55**
40	39	38	37	**51**	**53**	**56**	**61**
41	**42**	43	44	**52**	**57**	**60**	**62**
48	**47**	46	45	**58**	**59**	**63**	**64**

(a) Scan order, with two quadtrees

63	−34	49	10	5	18	−12	7
−31	23	14	−13	3	4	6	−1
−25	−7	−14	8	5	−7	3	9
−9	14	3	−12	4	−2	3	2
−5	9	−1	47	4	6	−2	2
3	0	−3	2	3	−2	0	4
2	−3	6	−4	3	6	3	6
5	11	5	6	0	3	−4	4

(b) Wavelet transform

+	−	+	*R*	*I*	*I*	•	•
I	*R*	*R*	*R*	*I*	*I*	•	•
R	*I*	•	•	•	•	•	•
R	*R*	•	•	•	•	•	•
•	•	*I*	+	•	•	•	•
•	•	*I*	*I*	•	•	•	•
•	•	•	•	•	•	•	•
•	•	•	•	•	•	•	•

(c) Threshold = 32

+	−	+	*R*	*I*	+	•	•
−	+	*R*	*R*	*I*	*I*	•	•
−	*R*	*R*	*R*	•	•	•	•
R	*R*	*R*	*R*	•	•	•	•
I	*I*	•	+	•	•	•	•
I	*I*	•	•	•	•	•	•
•	•	•	•	•	•	•	•
•	•	•	•	•	•	•	•

(d) Threshold = 16

Figure 6: First two stages of EZW. (a) 3-level scan order. (b) 3-level wavelet transform. (c) Stage 1, threshold = 32. (d) Stage 2, threshold = 16.

gions in image 7(c) produce insignificant values *in the same relative locations* (the child locations) in the 2nd vertical subband shown in image 7(d).

Likewise, there are uniformly grey regions in the same relative locations in the 1st vertical subband [see Fig. 7(f)]. Because the 2nd vertical subband in Fig. 7(d) is magnified by a factor of two in each dimension, and the 3rd vertical subband in 7(b) is magnified by a factor of four in each dimension, it follows that the common regions of grey background shown in these three vertical subbands are all zerotrees. Similar images could be shown for horizontal and diagonal subbands, and they would also indicate a large number of zerotrees.

The Lena image is typical of many images of natural scenes, and the above discussion gives some background for understanding how zerotrees arise in wavelet transforms. A more rigorous, statistical discussion can be found in Shapiro's paper [4].

Now that we have laid the foundations of zerotree encoding, we can complete our discussion of the EZW algorithm. The EZW algorithm simply consists of replacing the significance pass in the **Bit-plane encoding** procedure with the following step:

> **EZW Step 3** (*Significance pass*). Scan through insignificant values using baseline algorithm scan order. Test each value $w(m)$ as follows:
>
> ```
> If |w(m)| ≥ T_k, then
>     Output the sign of w(m)
>     Set w_Q(m) = T_k
> Else if |w(m)| < T_k then
>     Let w_Q(m) remain equal to 0
>     If m is at 1st level, then
>         Output I
>     Else
>         Search through quadtree having root m
>         If this quadtree is a zerotree, then
>             Output R
>         Else
>             Output I.
> ```
>
> During a search through a quadtree, values that were found to be significant at higher thresholds are treated as zeros. All descendants of a root of a zerotree are skipped in the rest of the scanning at this threshold.

(a) (b)

(c) (d)

(e) (f)

Figure 7: (a) 2nd all-lowpass subband. (b) 3rd vertical subband. (c) 1st all-lowpass subband. (d) 2nd vertical subband. (e) Original Lena. (f) 1st vertical subband.

As an example of the EZW method, consider the wavelet transform shown in Fig. 6(b), which will be scanned through using the scan order shown in Fig. 6(a). Suppose that the initial threshold is $T_0 = 64$. In the first loop, the threshold is $T_1 = 32$. The results of the first significance pass are shown in Fig. 6(c). The coder output after this first loop would be

$$+ - I\,R + R\,R\,R\,R\,I\,R\,R\,I\,I\,I\,I\,I + I\,I \tag{4}$$

corresponding to a quantized transform having just two values: ± 32. With $+32$ at each location marked by a plus sign in Fig. 6(c), and -32 at each location marked by a minus sign, and 0 at all other locations. In the second loop, with threshold $T_2 = 16$, the results of the significance pass are indicated in Fig. 6(d). Notice, in particular, that there is a symbol R at the position 11 in the scan order. That is because the plus sign which lies at a child location is from the previous loop, so it is treated as zero. Hence position 11 is at the root of a zerotree. There is also a refinement pass done in this second loop. The output from this second loop is then

$$- + R\,R\,R - R\,R\,R\,R\,R\,R\,R\,I\,I\,I + I\,I\,I\,I\,1\,0\,1\,0 \tag{5}$$

with corresponding quantized wavelet transform shown in Fig. 8(a). The MSE between this quantized transform and the original transform is 48.6875. This is a 78% reduction in error from the start of the method (when the quantized transform has all zero values).

A couple of final remarks are in order concerning the EZW method. First, it should be clear from the discussion above that the decoder, whose structure is outlined in Fig. 2 above, can reverse each of the steps of the coder and produce the quantized wavelet transform. It is standard practice for the decoder to then round the quantized values to the midpoints of the intervals that they were last found to belong to during the encoding process (i.e., add half of the last threshold used to their magnitudes). This generally reduces MSE. For instance, in the example just considered, if this rounding is done to the quantized transform in Fig. 8(a), then the result is shown in Fig. 8(b). The MSE is then 39.6875, a reduction of more than 18%. A good discussion of the theoretical justification for this rounding technique can be found in [2]. *This rounding method will be employed by all of the other algorithms that we shall discuss.*

Second, since we live in a digital world, it is usually necessary to transmit just bits. A simple encoding of the symbols of the EZW algorithm into bits

48	−32	48	0	0	16	0	0
−16	16	0	0	0	0	0	0
−16	0	0	0	0	0	0	0
0	0	0	0	0	0	0	0
0	0	0	32	0	0	0	0
0	0	0	0	0	0	0	0
0	0	0	0	0	0	0	0
0	0	0	0	0	0	0	0

(a)

56	−40	56	0	0	20	0	0
−24	24	0	0	0	0	0	0
−24	0	0	0	0	0	0	0
0	0	0	0	0	0	0	0
0	0	0	40	0	0	0	0
0	0	0	0	0	0	0	0
0	0	0	0	0	0	0	0
0	0	0	0	0	0	0	0

(b)

Figure 8: (a) Quantization at end of 2^{nd} stage, MSE = 48.6875. (b) After rounding to midpoints, MSE = 39.6875, reduction by more than 18%.

would be to use a code such as $P = 0\,1$, $N = 0\,0$, $R = 1\,0$, and $I = 1\,1$. Since the decoder can always infer precisely when the encoding of these symbols ends (the significance pass is complete), the encoding of refinement bits can simply be as single bits 0 and 1. This form of encoding is the fastest to perform, but it does not achieve the greatest compression. In [4], a lossless form of arithmetic coding was recommended in order to further compress the bit stream from the encoder.

1.3 SPIHT algorithm

The SPIHT algorithm is a highly refined version of the EZW algorithm. It was introduced in [5] and [6] by Said and Pearlman. Some of the best results—highest PSNR values for given compression ratios—for a wide variety of images have been obtained with SPIHT. Consequently, it is probably the most widely used wavelet-based algorithm for image compression, providing a basic standard of comparison for all subsequent algorithms.

SPIHT stands for *Set Partitioning in Hierarchical Trees.* The term *Hierarchical Trees* refers to the quadtrees that we defined in our discussion of EZW. *Set Partitioning* refers to the way these quadtrees divide up, partition,

the wavelet transform values at a given threshold. By a careful analysis of this partitioning of transform values, Said and Pearlman were able to greatly improve the EZW algorithm, significantly increasing its compressive power.

Our discussion of SPIHT will consist of three parts. First, we shall describe a modified version of the algorithm introduced in [5]. We shall refer to it as the *Spatial-orientation Tree Wavelet* (STW) algorithm. STW is essentially the SPIHT algorithm, the only difference is that SPIHT is slightly more careful in its organization of coding output. Second, we shall describe the SPIHT algorithm. It will be easier to explain SPIHT using the concepts underlying STW. Third, we shall see how well SPIHT compresses images.

The only difference between STW and EZW is that STW uses a different approach to encoding the zerotree information. STW uses a *state transition model.* From one threshold to the next, the locations of transform values undergo state transitions. This model allows STW to reduce the number of bits needed for encoding. Instead of code for the symbols R and I output by EZW to mark locations, the STW algorithm uses states I_R, I_V, S_R, and S_V and outputs code for state-transitions such as $I_R \to I_V$, $S_R \to S_V$, etc. To define the states involved, some preliminary definitions are needed.

For a given index m in the baseline scan order, define the set $\mathtt{D}(m)$ as follows. If m is either at the 1^{st} level or at the all-lowpass level, then $\mathtt{D}(m)$ is the empty set $\emptyset$. Otherwise, if m is at the j^{th} level for $j > 1$, then

$$\mathtt{D}(m) = \{\text{Descendents of index } m \text{ in quadtree with root } m\}.$$

The *significance function* $\mathcal{S}$ is defined by

$$\mathcal{S}(m) = \begin{cases} \max\limits_{n \in \mathtt{D}(m)} |w(n)|, & \text{if } \mathtt{D}(m) \neq \emptyset \\ \\ \infty, & \text{if } \mathtt{D}(m) = \emptyset. \end{cases}$$

With these preliminary definitions in hand, we can now define the states. For a given threshold T, the states I_R, I_V, S_R, and S_V are defined by

$$m \in I_R \quad \text{if and only if} \quad |w(m)| < T,\ \mathcal{S}(m) < T \tag{6}$$

$$m \in I_V \quad \text{if and only if} \quad |w(m)| < T,\ \mathcal{S}(m) \geq T \tag{7}$$

$$m \in S_R \quad \text{if and only if} \quad |w(m)| \geq T,\ \mathcal{S}(m) < T \tag{8}$$

$$m \in S_V \quad \text{if and only if} \quad |w(m)| \geq T,\ \mathcal{S}(m) \geq T. \tag{9}$$

In Fig. 9, we show the state transition diagram for these states when a

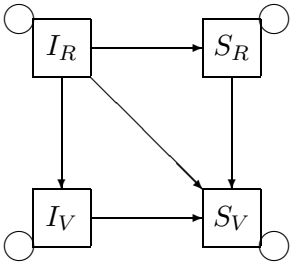

Figure 9: State transition diagram for STW

threshold is decreased from T to $T' < T$. Notice that once a location m arrives in state S_V, then it will remain in that state. Furthermore, there are only two transitions from each of the states I_V and S_R, so those transitions can be coded with one bit each. A simple binary coding for these state transitions is shown in Table 1.

Old\New	I_R	I_V	S_R	S_V
I_R	00	01	10	11
I_V		0		1
S_R			0	1
S_V				•

Table 1: Code for state transitions, • indicates that $S_V \rightarrow S_V$ transition is certain (hence no encoding needed).

Now that we have laid the groundwork for the STW algorithm, we can give its full description.

STW encoding

Step 1 (*Initialize*). Choose initial threshold, $T = T_0$, such that *all* transform values satisfy $|w(m)| < T_0$ and at least one transform value satisfies $|w(m)| \geq T_0/2$. Assign all indices for the L^{th} level, where L is the number of levels in the wavelet transform, to the *dominant list* (this includes all locations in the all-lowpass subband as well as the horizontal, vertical, and diagonal subbands at the L^{th} level). Set the *refinement list* of indices equal to the empty set.

Step 2 (*Update threshold*). Let $T_k = T_{k-1}/2$.

Step 3 (*Dominant pass*). Use the following procedure to scan through indices in the dominant list (which can change as the procedure is executed).

```
Do
    Get next index m in dominant list
    Save old state S_old = S(m, T_{k-1})
    Find new state S_new = S(m, T_k) using (6)-(9)
    Output code for state transition S_old → S_new
    If S_new ≠ S_old then do the following
        If S_old ≠ S_R and S_new ≠ I_V then
            Append index m to refinement list
            Output sign of w(m) and set w_Q(m) = T_k
        If S_old ≠ I_V and S_new ≠ S_R then
            Append child indices of m to dominant list
        If S_new = S_V then
            Remove index m from dominant list
Loop until end of dominant list
```

Step 4 (*Refinement pass*). Scan through indices m in the refinement list found with higher threshold values T_j, for $j < k$ (if $k = 1$ skip this step). For each value $w(m)$, do the following:

```
If |w(m)| ∈ [w_Q(m), w_Q(m) + T_k), then
    Output bit 0
Else if |w(m)| ∈ [w_Q(m) + T_k, w_Q(m) + 2T_k), then
    Output bit 1
    Replace value of w_Q(m) by w_Q(m) + T_k.
```

Step 5 (*Loop*). Repeat steps 2 through 4.

To see how STW works—and how it improves the EZW method—it helps to reconsider the example shown in Fig. 6. In Fig. 10, we show STW states for the wavelet transform in Fig. 6(b) using the same two thresholds as we used previously with EZW. It is important to compare the three quadtrees enclosed in the dashed boxes in Fig. 10 with the corresponding quadtrees in Figs. 6(c) and (d). There is a large savings in coding output for STW represented by these quadtrees. The EZW symbols for these three quadtrees

are $+\,I\,I\,I\,I$, $-\,I\,I\,I\,I$, and $+\,R\,R\,R\,R$. For STW, however, they are described by the symbols $+\,S_R$, $-\,S_R$, and $+\,S_R$, which is a substantial reduction in the information that STW needs to encode.

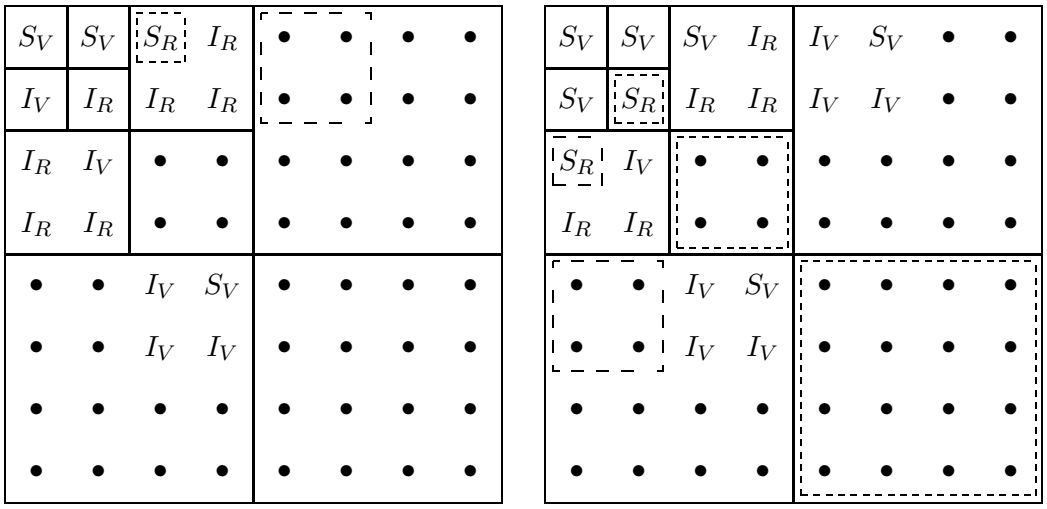

(a) Threshold = 32 (b) Threshold = 16

Figure 10: First two stages of STW for wavelet transform in Fig. 6.

There is not much difference between STW and SPIHT. The one thing that SPIHT does differently is to carefully organize the output of bits in the encoding of state transitions in Table 1, *so that only one bit is output at a time.* For instance, for the transition $I_R \rightarrow S_R$, which is coded as 1 0 in Table 1, SPIHT outputs a 1 first and then (after further processing) outputs a 0. Even if the bit budget is exhausted before the second bit can be output, the first bit of 1 indicates that there is a new significant value.

The SPIHT encoding process, as described in [6], is phrased in terms of pixel locations $[i, j]$ rather than indices m in a scan order. To avoid introducing new notation, and to highlight the connections between SPIHT and the other algorithms, EZW and STW, we shall rephrase the description of SPIHT from [6] in term of scanning indices. We shall also slightly modify the notation used in [6] in the interests of clarity.

First, we need some preliminary definitions. For a given set $\mathtt{I}$ of indices in the baseline scan order, the significance $\mathcal{S}_T[\mathtt{I}]$ of $\mathtt{I}$ relative to a threshold

T is defined by

$$\mathcal{S}_T[\mathtt{I}] = \begin{cases} 1, & \text{if } \max\limits_{n\in\mathtt{I}} |w(n)| \geq T \\ \\ 0, & \text{if } \max\limits_{n\in\mathtt{I}} |w(n)| < T. \end{cases} \tag{10}$$

It is important to note that, for the initial threshold T_0, we have $\mathcal{S}_{T_0}[\mathtt{I}] = 0$ for all sets of indices. If $\mathtt{I}$ is a set containing just a single index m, then for convenience we shall write $\mathcal{S}_T[m]$ instead of $\mathcal{S}_T[\{m\}]$.

For a succinct presentation of the method, we need the following definitions of sets of indices:

$$\begin{aligned} \mathtt{D}(m) &= \{\text{Descendent indices of the index } m\} \\ \mathtt{C}(m) &= \{\text{Child indices of the index } m\} \\ \mathtt{G}(m) &= \mathtt{D}(m) - \mathtt{C}(m) \\ &= \{\text{Grandchildren of } m, \text{ i.e., descendants which are not children}\}. \end{aligned}$$

In addition, the set $\mathtt{H}$ consists of indices for the L^{th} level, where L is the number of levels in the wavelet transform (this includes all locations in the all-lowpass subband as well as the horizontal, vertical, and diagonal subbands at the L^{th} level). It is important to remember that the indices in the all-lowpass subband have no descendants. If m marks a location in the all-lowpass subband, then $\mathtt{D}(m) = \emptyset$.

SPIHT keeps track of the states of sets of indices by means of three lists. They are the *list of insignificant sets* (`LIS`), the *list of insignificant pixels* (`LIP`), and the *list of significant pixels* (`LSP`). For each list a set is identified by a single index, in the `LIP` and `LSP` these indices represent the singleton sets $\{m\}$ where m is the identifying index. An index m is called either significant or insignificant, depending on whether the transform value $w(m)$ is significant or insignificant with respect to a given threshold. For the `LIS`, the index m denotes either $\mathtt{D}(m)$ or $\mathtt{G}(m)$. In the former case, the index m is said to be of type `D` and, in the latter case, of type `G`.

The following is pseudocode for the SPIHT algorithm. For simplicity, we shall write the significance function $\mathcal{S}_{T_k}$ as $\mathcal{S}_k$.

SPIHT encoding

Step 1 (*Initialize*). Choose initial threshold T_0 such that *all* transform values satisfy $|w(m)| < T_0$ and at least one value satisfies $|w(m)| \geq T_0/2$. Set `LIP` equal to `H`, set `LSP` equal to $\emptyset$, and set `LIS` equal to all the indices in `H` that have descendants (assigning them all type `D`).

Step 2 (*Update threshold*). Let $T_k = T_{k-1}/2$.

Step 3 (*Sorting pass*). Proceed as follows:

```
For each m in LIP do:
    Output S_k[m]
    If S_k[m] = 1 then
        Move m to end of LSP
        Output sign of w(m); set w_Q(m) = T_k
Continue until end of LIP
For each m in LIS do:
    If m is of type D then
        Output S_k[D(m)]
        If S_k[D(m)] = 1 then
            For each n ∈ C(m) do:
                Output S_k[n]
                If S_k[n] = 1 then
                    Append n to LSP
                    Output sign of w(n); set w_Q(n) = T_k
                Else If S_k[n] = 0 then
                    Append n to LIP
            If G(m) ≠ ∅ then
                Move m to end of LIS as type G
            Else
                Remove m from LIS
        Else If m is of type G then
            Output S_k[G(m)]
            If S_k[G(m)] = 1 then
                Append C(m) to LIS, all type D indices
                Remove m from LIS
Continue until end of LIS
```

Notice that the set `LIS` can undergo many changes during this procedure, it typically does not remain fixed throughout.

Step 4 (*Refinement pass*). Scan through indices m in `LSP` found with higher

threshold values T_j, for $j < k$ (if $k = 1$ skip this step). For each value $w(m)$, do the following:

```
If |w(m)| ∈ [w_Q(m), w_Q(m) + T_k), then
    Output bit 0
Else if |w(m)| ∈ [w_Q(m) + T_k, w_Q(m) + 2T_k), then
    Output bit 1
    Replace value of w_Q(m) by w_Q(m) + T_k.
```

Step 5 (*Loop*). Repeat steps 2 through 4.

It helps to carry out this procedure on the wavelet transform shown in Fig. 6. Then one can see that SPIHT simply performs STW *with the binary code for the states in Table 1 being output one bit at a time.*

Now comes the payoff. We shall see how well SPIHT performs in compressing images. To do these compressions we used the public domain SPIHT programs from [7]. In Fig. 11 we show several SPIHT compressions of the Lena image. The original Lena image is shown in Fig. 11(f). Five SPIHT compressions are shown with compression ratios of 128:1, 64:1, 32:1, 16:1, and 8:1.

There are several things worth noting about these compressed images. First, they were all produced from one file, the file containing the 1 bpp compression of the Lena image. By specifying a bit budget, a certain bpp value up to 1, the SPIHT decompression program will stop decoding the 1 bpp compressed file once the bit budget is exhausted. This illustrates the embedded nature of SPIHT.

Second, the rapid convergence of the compressed images to the original is nothing short of astonishing. Even the 64: 1 compression in Fig. 11(b) is almost indistinguishable from the original. A close examination of the two images is needed in order to see some differences, e.g., the blurring of details in the top of Lena's hat. The image in (b) would be quite acceptable for some applications, such as the first image in a sequence of video telephone images or as a thumbnail display within a large archive.

Third, notice that the 1 bpp image has a 40.32 dB PSNR value and is virtually indistinguishable—even under very close examination—from the original. Here we find that SPIHT is able to exceed the simple thresholding compression we first discussed (see Fig. 3). For reasons of space, we cannot show SPIHT compressions of many test images, so in Table 2 we give PSNR

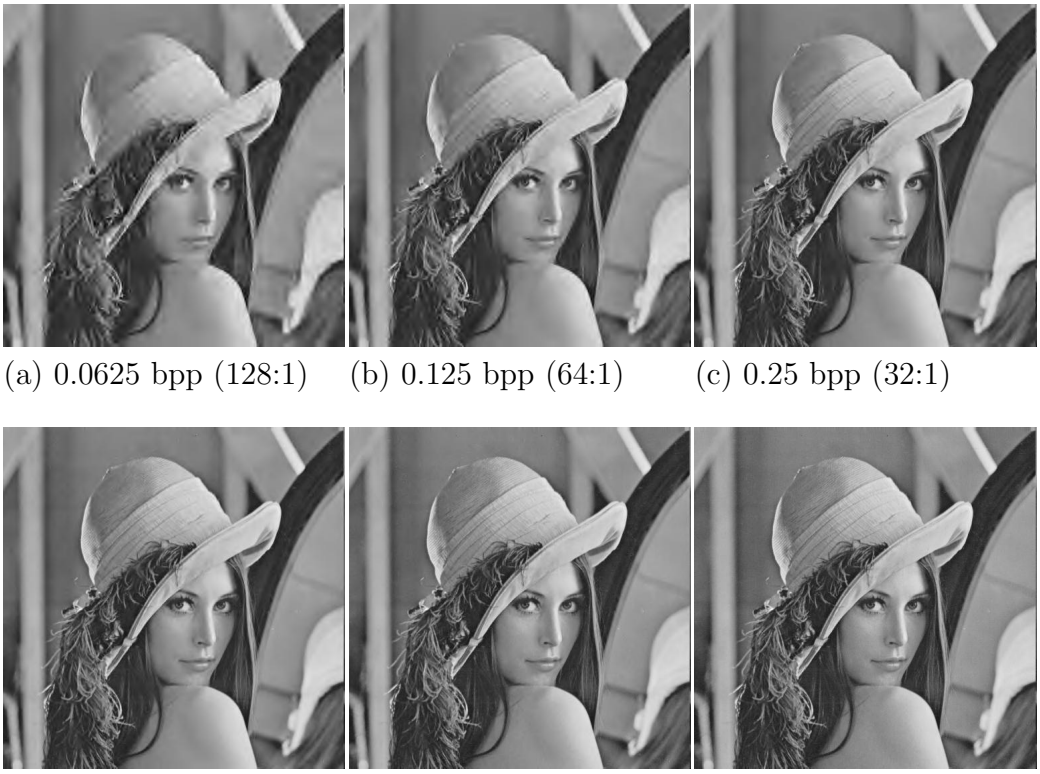

(a) 0.0625 bpp (128:1) (b) 0.125 bpp (64:1) (c) 0.25 bpp (32:1)

(d) 0.5 bpp (16:1) (e) 1.0 bpp (8:1) (f) Original, 8 bpp

Figure 11: SPIHT compressions of Lena image. PSNR values: (a) 27.96 dB. (b) 30.85 dB. (c) 33.93 dB. (d) 37.09 dB. (e) 40.32 dB.

values for several test images [8]. These data show that SPIHT produces higher PSNR values than the two other algorithms that we shall describe below. SPIHT is well-known for its superior performance when PSNR is used as the error measure. High PSNR values, however, are not the sole criteria for the performance of lossy compression algorithms. We shall discuss other criteria below.

Fourth, these SPIHT compressed images were obtained using SPIHT's arithmetic compression option. The method that SPIHT uses for arithmetic compression is quite involved and space does not permit a discussion of the details here. Some details are provided in [9].

Finally, it is interesting to compare SPIHT compressions with compres-

Image/Method	SPIHT	WDR	ASWDR
Lena, 0.5 bpp	**37.09**	36.45	36.67
Lena, 0.25 bpp	**33.85**	33.39	33.64
Lena, 0.125 bpp	**30.85**	30.42	30.61
Goldhill, 0.5 bpp	**33.10**	32.70	32.85
Goldhill, 0.25 bpp	**30.49**	30.33	30.34
Goldhill, 0.125 bpp	**28.39**	28.25	28.23
Barbara, 0.5 bpp	**31.29**	30.68	30.87
Barbara, 0.25 bpp	**27.47**	26.87	27.03
Barbara, 0.125 bpp	**24.77**	24.30	24.52
Airfield, 0.5 bpp	**28.57**	28.12	28.36
Airfield, 0.25 bpp	**25.90**	25.49	25.64
Airfield, 0.125 bpp	**23.68**	23.32	23.50

Table 2: PSNR values, *with* arithmetic compression

sions obtained with the JPEG method.[2] The JPEG method is a sophisticated implementation of block Discrete Cosine Transform encoding [10]. It is used extensively for compression of images, especially for transmission over the Internet. In Fig. 12, we compare compressions of the Lena image obtained with JPEG and with SPIHT at three different compression ratios. (JPEG does not allow for specifying the bpp value in advance; the 59:1 compression was the closest we could get to 64:1.) It is clear from these images that SPIHT is far superior to JPEG. It is better both in perceptual quality and in terms of PSNR. Notice, in particular, that the 59:1 JPEG compression is very distorted (exhibiting "blocking" artifacts stemming from coarse quantization within the blocks making up the block DCT used by JPEG). The SPIHT compression, even at the slightly higher ratio of 64:1, exhibits none of these objectionable features. In fact, for quick transmission of a thumbnail image (say, as part of a much larger webpage), this SPIHT compression would be quite acceptable. The 32:1 JPEG image might be acceptable for some applications, but it also contains some blocking artifacts. The 32:1 SPIHT compression is almost indistinguishable (at these image sizes) from the original Lena image. The 16:1 compressions for both methods are nearly

[2]JPEG stands for Joint Photographic Experts Group, a group of engineers who developed this compression method.

indistinguishable. In fact, they are both nearly indistinguishable from the original Lena image.

Although we have compared JPEG with SPIHT using only one image, the results we have found are generally valid. SPIHT compressions are superior to JPEG compressions both in perceptual quality and in PSNR values. In fact, all of the wavelet-based image compression techniques that we discuss here are superior to JPEG. Hence, we shall not make any further comparisons with the JPEG method.

(a) JPEG 59:1 (b) JPEG 32:1 (c) JPEG 16:1

(d) SPIHT 64:1 (e) SPIHT 32:1 (f) SPIHT 16:1

Figure 12: Comparison of JPEG and SPIHT compressions of Lena image. PSNR values: (a) 24.16 dB. (b) 30.11 dB. (c) 34.12 dB. (d) 30.85 dB. (e) 33.93 dB. (f) 37.09 dB.

1.4 WDR Algorithm

One of the defects of SPIHT is that it only *implicitly* locates the position of significant coefficients. This makes it difficult to perform operations, such as region selection on compressed data, which depend on the exact position of significant transform values. By *region selection*, also known as *region of interest* (ROI), we mean selecting a portion of a compressed image which requires increased resolution. This can occur, for example, with a portion of a low resolution medical image that has been sent at a low bpp rate in order to arrive quickly.

Such compressed data operations are possible with the *Wavelet Difference Reduction* (WDR) algorithm of Tian and Wells [11]–[13]. The term *difference reduction* refers to the way in which WDR encodes the locations of significant wavelet transform values, which we shall describe below. Although WDR will not typically produce higher PSNR values than SPIHT (see Table 2), we shall see that WDR can produce perceptually superior images, especially at high compression ratios.

The only difference between WDR and the **Bit-plane encoding** described above is in the significance pass. In WDR, the output from the significance pass consists of the signs of significant values along with sequences of bits which concisely describe the precise locations of significant values. The best way to see how this is done is to consider a simple example.

Suppose that the significant values are $w(2) = +34.2$, $w(3) = -33.5$, $w(7) = +48.2$, $w(12) = +40.34$, and $w(34) = -54.36$. The indices for these significant values are 2, 3, 7, 12, and 34. Rather than working with these values, WDR works with their successive differences: 2, 1, 4, 5, 22. In this latter list, the first number is the *starting index* and each successive number is the *number of steps* needed to reach the next index. The binary expansions of these successive differences are $(10)_2$, $(1)_2$, $(100)_2$, $(101)_2$, and $(10110)_2$. Since the most significant bit for each of these expansions is always 1, this bit can be dropped and the signs of the significant transform values can be used instead as separators in the symbol stream. The resulting symbol stream for this example is then $+0 - +00 + 01 - 0110$.

When this most significant bit is dropped, we shall refer to the binary expansion that remains as the *reduced binary expansion*. Notice, in particular, that the reduced binary expansion of 1 is empty. The reduced binary expansion of 2 is just the 0 bit, the reduced binary expansion of 3 is just the 1 bit, and so on.

The WDR algorithm simply consists of replacing the significance pass in the **Bit-plane encoding** procedure with the following step:

WDR Step 3 (*Significance pass*). Perform the following procedure on the insignificant indices in the baseline scan order:

```
Initialize step-counter C = 0
Let C_old = 0
Do
    Get next insignificant index m
    Increment step-counter C by 1
    If |w(m)| ≥ T_k then
        Output sign w(m) and set w_Q(m) = T_k
        Move m to end of sequence of significant indices
        Let n = C − C_old
        Set C_old = C
        If n > 1 then
            Output reduced binary expansion of n
    Else if |w(m)| < T_k then
        Let w_Q(m) retain its initial value of 0.
Loop until end of insignificant indices
Output end-marker
```

The output for the end-marker is a plus sign, followed by the reduced binary expansion of $n = C + 1 - C_{\text{old}}$, and a final plus sign.

It is not hard to see that WDR is of no greater computational complexity than SPIHT. For one thing, WDR does not need to search through quadtrees as SPIHT does. The calculations of the reduced binary expansions adds some complexity to WDR, but they can be done rapidly with bit-shift operations. As explained in [11]–[13], the output of the WDR encoding can be arithmetically compressed. The method that they describe is based on the elementary arithmetic coding algorithm described in [14]. This form of arithmetic coding is substantially less complex (at the price of poorer performance) than the arithmetic coding employed by SPIHT.

As an example of the WDR algorithm, consider the scan order and wavelet transform shown in Fig. 6. For the threshold $T_1 = 32$, the significant values

are $w(1) = 63$, $w(2) = -34$, $w(5) = 49$, and $w(36) = 47$. The output of the WDR significance pass will then be the following string of symbols:

$$+\ -\ +1\ +\ 1\,1\,1\,1\ +\ 1\,1\,0\,1+$$

which compares favorably with the EZW output in Eq. (4). The last six symbols are the code for the end-marker. For the threshold $T_2 = 16$, the new significant values are $w(3) = -31$, $w(4) = 23$, $w(9) = -25$, and $w(24) = 18$. Since the previous indices 1, 2, 5, and 36, are removed from the sequence of insignificant indices, the values of n in the WDR significance pass will be 1, 1, 4, and 15. In this case, the value of n for the end-marker is 40. Adding on the four refinement bits, which are the same as in Eq. (5), the WDR output for this second threshold is

$$-\ +\ -0\,0\ +\ 1\,1\,1\ +\ 0\,1\,0\,0\,0\ +\ 1\,0\,1\,0$$

which is also a smaller output than the corresponding EZW output. It is also clear that, for this simple case, WDR does *not* produce as compact an output as STW does.

As an example of WDR performance for a natural image, we show in Fig. 13 several compressions of the Lena image. These compressions were produced with the free software [15].

There are a couple things to observe about these compressions. First, the PSNR values are lower than for SPIHT. This is typically the case. In Table 2 we compare PSNR values for WDR and for SPIHT on several images at various compression ratios. In every case, SPIHT has higher PSNR values.

Second, at high compression ratios, the visual quality of WDR compressions of Lena are superior to those of SPIHT. For example, the 0.0625 bpp and 0.125 bpp compressions have higher resolution with WDR. This is easier to see if the images are magnified as in Fig. 14. At 0.0625 bpp, the WDR compression does a better job in preserving the shape of Lena's nose and in retaining some of the striping in the band around her hat. Similar remarks apply to the 0.125 bpp compressions. SPIHT, however, does a better job in preserving parts of Lena's eyes. These observations point to the need for an objective, quantitative measure of image quality.

There is no universally accepted objective measure for image quality. We shall now describe a simple measure that we have found useful. There is some evidence that the visual system of humans concentrates on analyzing edges in images [16], [17]. To produce an image that retains only edges, we proceed as

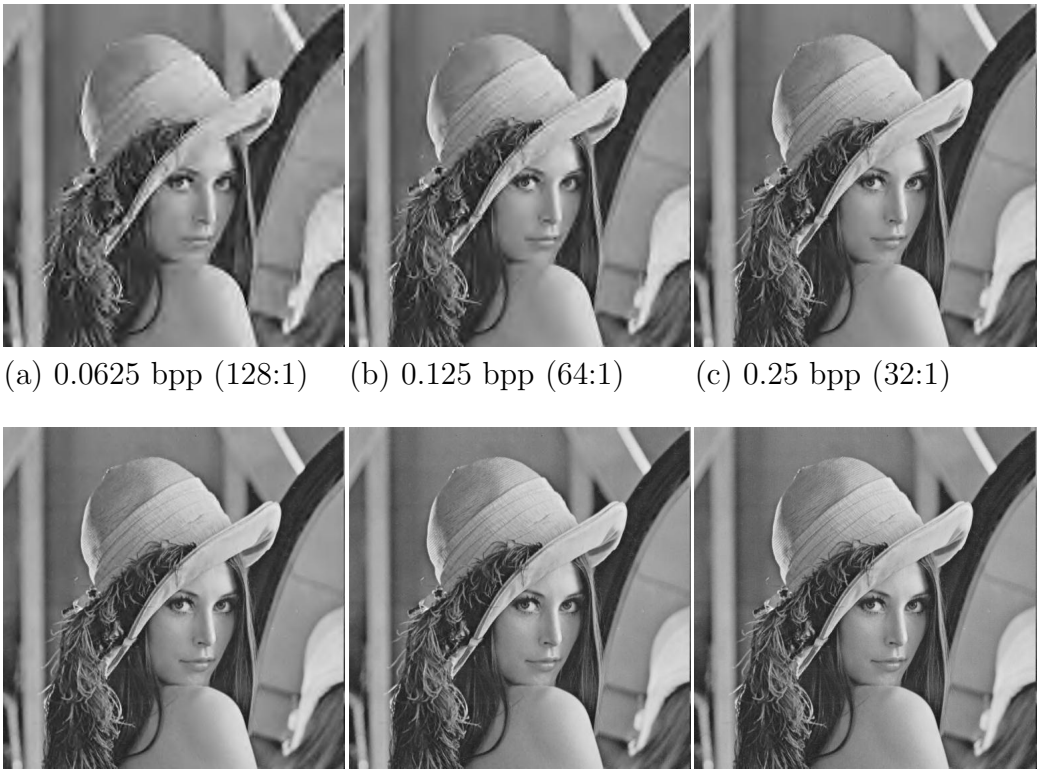

(a) 0.0625 bpp (128:1) (b) 0.125 bpp (64:1) (c) 0.25 bpp (32:1)

(d) 0.5 bpp (16:1) (e) 1.0 bpp (8:1) (f) Original, 8 bpp

Figure 13: WDR compressions of Lena image. PSNR values: (a) 27.63 dB. (b) 30.42 dB. (c) 33.39 dB. (d) 36.45 dB. (e) 39.62 dB.

follows. First, a 3-level Daub 9/7 transform of an image f is created. Second, the all-lowpass subband is subtracted away from this transform. Third, an inverse transform is performed on the remaining part of the transform. This produces a highpass filtered image, which exhibits edges from the image f. A similar highpass filtered image is created from the compressed image. Both of these highpass filtered images have mean values that are approximately zero. We define the *edge correlation* γ_3 by

$$\gamma_3 = \frac{\sigma_c}{\sigma_o}$$

where σ_c denotes the standard deviation of the values of the highpass filtered version of the compressed image, and σ_o denotes the standard deviation of the values of the highpass filtered version of the original image. Thus γ_3 measures

(a) Original (b) SPIHT, 0.0625 bpp (c) WDR, 0.0625 bpp

(d) Original (e) SPIHT, 0.125 bpp (f) WDR, 0.125 bpp

Figure 14: SPIHT and WDR compressions of Lena at low bpp.

how well the compressed image captures the variation of edge details in the original image.

Using this edge correlation measure, we obtained the results shown in Table 3. In every case, the WDR compressions exhibit higher edge correlations than the SPIHT compressions. These numerical results are also consistent with the increased preservation of details within WDR images, and with the informal reports of human observers.

Although WDR is simple, competitive with SPIHT in PSNR values, and often provides better perceptual results, there is still room for improvement. We now turn to a recent enhancement of the WDR algorithm.

Image/Method	SPIHT	WDR	ASWDR
Lena, 0.5 bpp	.966	.976	**.978**
Lena, 0.25 bpp	.931	.946	**.951**
Lena, 0.125 bpp	.863	.885	**.894**
Goldhill, 0.5 bpp	.920	.958	**.963**
Goldhill, 0.25 bpp	.842	.870	**.871**
Goldhill, 0.125 bpp	.747	**.783**	.781
Barbara, 0.5 bpp	.932	.955	**.959**
Barbara, 0.25 bpp	.861	.894	**.902**
Barbara, 0.125 bpp	.739	.767	**.785**
Airfield, 0.5 bpp	.922	**.939**	.937
Airfield, 0.25 bpp	.857	.871	**.878**
Airfield, 0.125 bpp	.766	.790	**.803**

Table 3: Edge correlations, *with* arithmetic compression

1.5 ASWDR algorithm

One of the most recent image compression algorithms is the *Adaptively Scanned Wavelet Difference Reduction* (ASWDR) algorithm of Walker [18]. The adjective *adaptively scanned* refers to the fact that this algorithm modifies the scanning order used by WDR in order to achieve better performance.

ASWDR adapts the scanning order so as to predict locations of new significant values. If a prediction is correct, then the output specifying that location will just be the sign of the new significant value—the reduced binary expansion of the number of steps will be empty. Therefore a good prediction scheme will significantly reduce the coding output of WDR.

The prediction method used by ASWDR is the following: *If $w(m)$ is significant for threshold T, then the values of the children of m are predicted to be significant for half-threshold $T/2$.* For many natural images, this prediction method is a reasonably good one. As an example, in Fig. 15 we show two vertical subbands for a Daub 9/7 wavelet transform of the Lena image. The image in Fig. 15(a) is of those significant values in the 2^{nd} level vertical subband for a threshold of 16 (significant values shown in white). In Fig. 15(b), we show the *new* significant values in the 1^{st} vertical subband for the half-threshold of 8. Notice that there is a great deal of similarity in the two images. Since the image in Fig. 15(a) is magnified by two in each dimen-

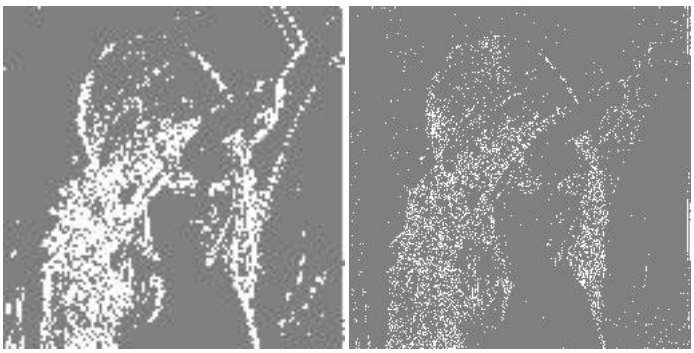

(a) (b)

Figure 15: (a) Significant values, 2nd vertical subband, threshold 16. (b) *New* significant values, 1st vertical subband, threshold 8.

sion, its white pixels actually represent the predictions for the locations of new significant values in the 1st vertical subband. Although these predictions are not perfectly accurate, there is a great deal of overlap between the two images. Notice also how the locations of significant values are highly correlated with the location of edges in the Lena image. The scanning order of ASWDR dynamically adapts to the locations of edge details in an image, and this enhances the resolution of these edges in ASWDR compressed images.

A complete validation of the prediction method just described would require assembling statistics for a large number of different subbands, different thresholds, and different images. Rather than attempting such an *a priori* argument (see [19]), we shall instead argue from an *a posteriori* standpoint. We shall present statistics that show that the prediction scheme employed by ASWDR does, in fact, encode more significant values than are encoded by WDR for a number of different images. As the pseudocode presented below will show, the only difference between ASWDR and WDR is in the predictive scheme employed by ASWDR to create new scanning orders. Consequently, if ASWDR typically encodes more values than WDR does, this must be due to the success of the predictive scheme.

In Table 4 we show the numbers of significant values encoded by WDR and ASWDR for four different images. In almost every case, ASWDR was able to encode more values than WDR. This gives an *a posteriori* validation of the predictive scheme employed by ASWDR.

We now present the pseudocode description of ASWDR encoding. Notice

Image\Method	WDR	ASWDR	% increase
Lena, 0.125 bpp	5,241	5,458	4.1%
Lena, 0.25 bpp	10,450	11,105	6.3%
Lena, 0.5 bpp	20,809	22,370	7.5%
Goldhill, 0.125 bpp	5,744	5,634	−1.9%
Goldhill, 0.25 bpp	10,410	10,210	−1.9%
Goldhill, 0.5 bpp	22,905	23,394	2.1%
Barbara, 0.125 bpp	5,348	5,571	4.2%
Barbara, 0.25 bpp	11,681	12,174	4.2%
Barbara, 0.5 bpp	23,697	24,915	5.1%
Airfield, 0.125 bpp	5,388	5,736	6.5%
Airfield, 0.25 bpp	10,519	11,228	6.7%
Airfield, 0.5 bpp	19,950	21,814	9.3%

Table 4: Number of significant values encoded, *no* arithmetic coding

that the significance pass portion of this procedure is the same as the WDR significance pass described above, and that the refinement pass is the same as for **Bit-plane encoding** (hence the same as for WDR). The one new feature is the insertion of a step for creating a new scanning order.

ASWDR encoding

Step 1 (*Initialize*). Choose initial threshold, $T = T_0$, such that *all* transform values satisfy $|w(m)| < T_0$ and at least one transform value satisfies $|w(m)| \geq T_0/2$. Set the initial scan order to be the baseline scan order.

Step 2 (*Update threshold*). Let $T_k = T_{k-1}/2$.

Step 3 (*Significance pass*). Perform the following procedure on the insignificant indices in the scan order:

```
Initialize step-counter C = 0
Let C_old = 0
Do
    Get next insignificant index m
    Increment step-counter C by 1
    If |w(m)| ≥ T_k then
```

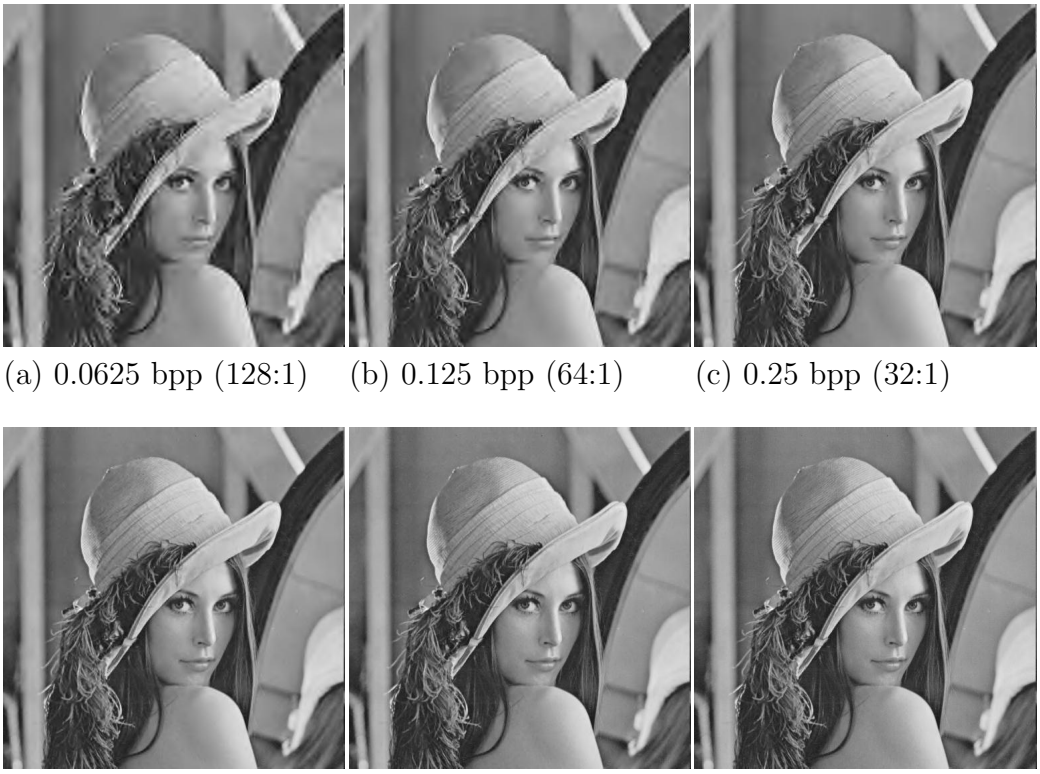

(a) 0.0625 bpp (128:1) (b) 0.125 bpp (64:1) (c) 0.25 bpp (32:1)

(d) 0.5 bpp (16:1) (e) 1.0 bpp (8:1) (f) Original, 8 bpp

Figure 16: ASWDR compressions of Lena image. PSNR values: (a) 27.73 dB. (b) 30.61 dB. (c) 33.64 dB. (d) 36.67 dB. (e) 39.90 dB.

```
            Output sign w(m) and set w_Q(m) = T_k
            Move m to end of sequence of significant indices
            Let n = C − C_old
            Set C_old = C
            If n > 1 then
                Output reduced binary expansion of n
        Else if |w(m)| < T_k then
            Let w_Q(m) retain its initial value of 0.
    Loop until end of insignificant indices
    Output end-marker as per WDR Step 3
```

Step 4 (*Refinement pass*). Scan through significant values found with higher threshold values T_j, for $j < k$ (if $k = 1$ skip this step). For each significant value $w(m)$, do the following:

```
If |w(m)| ∈ [w_Q(m), w_Q(m) + T_k), then
    Output bit 0
Else if |w(m)| ∈ [w_Q(m) + T_k, w_Q(m) + 2T_k), then
    Output bit 1
    Replace value of w_Q(m) by w_Q(m) + T_k.
```

Step 5 (*Create new scan order*). For each level j in the wavelet transform (except for $j = 1$), scan through the significant values using the old scan order. The initial part of the new scan order at level $j - 1$ consists of the indices for insignificant values corresponding to the child indices of these level j significant values. Then, scan again through the insignificant values at level j using the old scan order. Append to the initial part of the new scan order at level $j - 1$ the indices for insignificant values corresponding to the child indices of these level j significant values. *Note:* No change is made to the scan order at level L, where L is the number of levels in the wavelet transform.

Step 6 (*Loop*). Repeat steps 2 through 5.

The creation of the new scanning order only adds a small degree of complexity to the original WDR algorithm. Moreover, ASWDR retains all of the attractive features of WDR: simplicity, progressive transmission capability, and ROI capability.

In Fig. 16 we show how ASWDR performs on the Lena image. The PSNR values for these images are slightly better than those for WDR, and almost as good as those for SPIHT. More importantly, the perceptual quality of ASWDR compressions are better than SPIHT compressions and slightly better than WDR compressions. This is especially true at high compression ratios. In Fig. 17 we show magnifications of 128:1 and 64:1 compressions of the Lena image. The ASWDR compressions better preserve the shape of Lena's nose, and details of her hat, and show less distortion along the side of her left cheek (especially for the 0.125 bpp case). These subjective observations are borne out by the edge correlations in Table 3. In almost every case, the ASWDR compressions produce slightly higher edge correlation values.

As a further example of the superior performance of ASWDR at high compression ratios, in Fig. 18 we show compressions of the Airfield image at

(a) SPIHT (b) WDR (c) ASWDR

(d) SPIHT (e) WDR (f) ASWDR

Figure 17: SPIHT, WDR, and ASWDR compressions of Lena at low bpp. (a)–(c) 0.0625 bpp, 128:1. (d)–(f) 0.125 bpp, 64:1.

128:1. The WDR and ASWDR algorithms preserve more of the fine details in the image. Look especially along the top of the images: SPIHT erases many fine details such as the telephone pole and two small square structures to the right of the thin black rectangle. These details are preserved, at least partially, by both WDR and ASWDR. The ASWDR image does the best job in retaining some structure in the telephone pole. ASWDR is also superior in preserving the structure of the swept-back winged aircraft, especially its thin nose, located to the lower left of center. These are only a few of the many details in the airplane image which are better preserved by ASWDR.

As quantitative support for the superiority of ASWDR in preserving edge details, we show in Table 5 the values for three different edge correlations γ_k, $k = 3$, 4, and 5. Here k denotes how many levels in the Daub 9/7 wavelet

(a) Original (b) SPIHT

(c) WDR (d) ASWDR

Figure 18: Comparisons of 128:1 compressions of airfield image

transform were used. A higher value of k means that edge detail at lower resolutions was considered in computing the edge correlation. These edge correlations show that ASWDR is superior over several resolution levels in preserving edges in the airfield image at the low bit rate of 0.0625 bpp.

High compression ratio images like these are used in reconnaissance and in medical applications, where fast transmission and ROI (region selection) are employed, as well as multi-resolution detection. The WDR and ASWDR algorithms do allow for ROI while SPIHT does not. Furthermore, their superior performance in displaying edge details at low bit rates facilitates multi-resolution detection.

Further research is being done on improving the ASWDR algorithm. One important enhancement will be the incorporation of an improved predictive

Corr./Method	SPIHT	WDR	ASWDR
γ_3	.665	.692	**.711**
γ_4	.780	.817	**.827**
γ_5	.845	.879	**.885**

Table 5: Edge correlations for 128:1 compressions of Airfield image

scheme, based on weighted values of neighboring transform magnitudes as described in [19].

1.6 Lossless compression

A novel aspect of the compression/decompression methods diagrammed in Figs. 1 and 2 is that *integer-to-integer* wavelet transforms can be used in place of the ordinary wavelet transforms (such as Daub 9/7) described so far. An integer-to-integer wavelet transform produces an integer-valued transform from the grey-scale, integer-valued image [20]. Since n loops in **Bit-plane encoding** reduces the quantization error to less than $T_0/2^n$, it follows that *once* 2^n *is greater than* T_0*, there will be zero error.* In other words, the bit-plane encoded transform will be exactly the same as the original wavelet transform, hence lossless encoding is achieved (with progressive transmission as well). Of course, for many indices, the zero error will occur sooner than with the maximum number of loops n. Consequently, some care is needed in order to efficiently encode the minimum number of bits in each binary expansion. A discussion of how SPIHT is adapted to achieve lossless encoding can be found in [9]. The algorithms WDR and ASWDR can also be adapted in order to achieve lossless encoding, but public versions of such adaptations are not yet available. (When they are released, they will be accessible at [15].)

1.7 Color images

Following the standard practice in image compression research, we have concentrated here on methods of compressing grey-scale images. For color images, this corresponds to compressing the *intensity* portion of the image. That is, if the color image is a typical RGB image, with 8 bits for Red, 8 bits for Green, and 8 bits for Blue, then the intensity I is defined by

$I = (R + B + G)/3$, which rounds to an 8-bit grey-scale image. The human eye is most sensitive to variations in intensity, so the most difficult part of compressing a color image lies in the compressing of the intensity. Usually, the two color "channels" are denoted Y and C and are derived from the R, G, and B values [21]. Much greater compression can be done on the Y and C versions of the image, since the human visual system is much less sensitive to variations in these two variables. Each of the algorithms described above can be modified so as to compress color images. For example, the public domain SPIHT coder [7] does provide programs for compressing color images. For reasons of space, we cannot describe compression of color images in any more detail.

1.8 Other compression algorithms

There are a wide variety of wavelet-based image compression algorithms besides the ones that we focused on here. Some of the most promising are algorithms that minimize the amount of memory which the encoder and/or decoder must use, see [22] and [23]. A new algorithm which is embedded and which minimizes PSNR is described in [24]. Many other algorithms are cited in the review article [1]. In evaluating the performance of any new image compression algorithm, one must take into account not only PSNR values, but also consider the following factors: (1) perceptual quality of the images (edge correlation values can be helpful here), (2) whether the algorithm allows for progressive transmission, (3) the complexity of the algorithm (including memory usage), and (4) whether the algorithm has ROI capability.

References

[1] G.M. Davis, A. Nosratinia. Wavelet-based Image Coding: An Overview. *Applied and Computational Control, Signals and Circuits,* Vol. 1, No. 1, 1998.

[2] S. Mallat. *A Wavelet Tour of Signal Processing.* Academic Press, New York, NY, 1998.

[3] M. Antonini, M. Barlaud, P. Mathieu, I. Daubechies. Image coding using wavelet transform. *IEEE Trans. Image Proc.,* Vol. 5, No. 1, pp. 205-220, 1992.

[4] J.M. Shapiro. Embedded image coding using zerotrees of wavelet coefficients. *IEEE Trans. Signal Proc.,* Vol. 41, No. 12, pp. 3445–3462, 1993.

[5] A. Said, W.A. Pearlman. Image compression using the spatial-orientation tree. *IEEE Int. Symp. on Circuits and Systems,* Chicago, IL, pp. 279–282, 1993.

[6] A. Said, W.A. Pearlman. A new, fast, and efficient image codec based on set partitioning in hierarchical trees. *IEEE Trans. on Circuits and Systems for Video Technology,* Vol. 6, No. 3, pp. 243–250, 1996.

[7] SPIHT programs can be downloaded from `ftp://ipl.rpi.edu/pub/`.

[8] Go to `ftp://ipl.rpi.edu/pub/image/still/usc/gray/` for Lena, Goldhill, and Barbara. Go to `http://www.image.cityu.edu.hk/imagedb/` for Airfield.

[9] A. Said, W.A. Pearlman. An image multi-resolution representation for lossless and lossy image compression. *IEEE Trans. Image Proc.,* Vol. 5, No. 9, pp. 1303–1310, 1996.

[10] G.K. Wallace. The JPEG still picture compression standard. *Comm. of the ACM,* Vol. 34, No. 4, pp. 30–44, 1991.

[11] J. Tian, R.O. Wells, Jr. A lossy image codec based on index coding. *IEEE Data Compression Conference, DCC '96,* page 456, 1996.

[12] J. Tian, R.O. Wells, Jr. Embedded image coding using wavelet-difference-reduction. *Wavelet Image and Video Compression,* P. Topiwala, ed., pp. 289–301. Kluwer Academic Publ., Norwell, MA, 1998.

[13] J. Tian, R.O. Wells, Jr. Image data processing in the compressed wavelet domain. *3rd International Conference on Signal Processing Proc.,* B. Yuan and X. Tang, Eds., pp. 978–981, Beijing, China, 1996.

[14] I. Witten, R. Neal, J. Cleary. Arithmetic coding for data compression. *Comm. of the ACM,* Vol. 30, No. 6, pp. 1278–1288, 1986.

[15] WDR and ASWDR compressors are part of the FAWAV software package at `http://www.crcpress.com/edp/download/fawav/fawav.htm/`

[16] D. Marr, *Vision.* W.H. Freeman, San Francisco, CA, 1982.

[17] M.G. Ramos, S.S. Hemami, Activity selective SPIHT coding. *Proc. SPIE 3653, Visual Communications and Image Processing '99,* San Jose, CA, Jan. 1999. See also errata for this paper at `http://foulard.ee.cornell.edu/marcia/asspiht2.html`.

[18] J.S. Walker. A lossy image codec based on adaptively scanned wavelet difference reduction. Submitted to *Optical Engineering.*

[19] R.W. Buccigrossi, E.P. Simoncelli, Image compression via joint statistical characterization in the wavelet domain. *IEEE Trans. on Image Proc.,* Vol. 8, No. 12, 1999.

[20] A.R. Calderbank, I. Daubechies, W. Sweldens, B.-L. Yeo, Wavelet transforms that map integers to integers. *Applied and Computational Harmonic Analysis,* Vol. 5, No. 3, pp. 332-369, 1998.

[21] J.C. Russ, *The Image Processing Handbook.* CRC Press, Boca Raton, FL, 1995.

[22] A. Islam, W.A. Pearlman, An embedded and efficient low-complexity hierarchical image coder. *Proc. SPIE 3653, Visual Communications and Image Processing '99,* San Jose, CA, Jan. 1999.

[23] H. Malvar, Progressive wavelet coding of images. *Proc. of IEEE Data Compression Conference,* Salt Lake City, UT, pp. 336–343, March, 1999.

[24] J. Li, S. Lei, An embedded still image coder with rate-distortion optimization. *IEEE Trans. on Image Proc.,* Vol. 8, No. 7, pp. 913–924, 1999.